

**Title: The complete structure of the 55S mammalian mitochondrial ribosome**

**Authors:** Basil J. Greber<sup>1,\*</sup>, Philipp Bieri<sup>1,\*</sup>, Marc Leibundgut<sup>1,\*</sup>, Alexander Leitner<sup>2</sup>, Ruedi Aebersold<sup>2,3</sup>, Daniel Boehringer<sup>1</sup>, Nenad Ban<sup>1,†</sup>

\* These authors contributed equally to this work.

**Affiliations:** <sup>1</sup> Department of Biology, Institute of Molecular Biology and Biophysics, Otto-Stern-Weg 5, ETH Zurich, CH-8093 Zurich, Switzerland

<sup>2</sup> Department of Biology, Institute of Molecular Systems Biology, Auguste-Piccard-Hof 1, ETH Zurich, CH-8093 Zurich, Switzerland

<sup>3</sup> Faculty of Science, University of Zurich, CH-8057 Zurich, Switzerland

† Corresponding author. E-mail: ban@mol.biol.ethz.ch

**One sentence summary:** The structure of the entire mammalian 55S mitoribosome has been determined by cryo-electron microscopy and chemical crosslinking/mass spectrometry, revealing the detailed structure of the small mitoribosomal subunit and its interactions with mRNA and tRNA ligands.

**Abstract:** Mammalian mitochondrial ribosomes synthesize mitochondrially encoded membrane proteins that are critical for mitochondrial function. Here we present the complete atomic structure of the porcine 55S mitoribosome at 3.8 Å resolution by cryo-electron microscopy and chemical crosslinking/mass spectrometry. The structure of the 28S subunit in the complex was resolved at 3.6 Å resolution by focused alignment, which allowed building of a detailed atomic structure including all of its 15 mitoribosomal-specific proteins. The structure reveals the intersubunit contacts in the 55S mitoribosome, the molecular architecture of the mitoribosomal mRNA binding channel and its interaction with tRNAs, and provides insight into the highly specialized mechanism of mRNA recruitment to the 28S subunit. Furthermore, the structure contributes to a mechanistic understanding of aminoglycoside ototoxicity.

**Main Text:** Mitochondria are eukaryotic cellular organelles specialized for energy conversion and ATP production. Because they originated by endosymbiosis from  $\alpha$ -proteobacteria (1), they still contain the machinery required to express the genetic information encoded on their highly reduced genome, including mitochondrial ribosomes (mitoribosomes). Mammalian 55S mitoribosomes, composed of the 28S small and 39S large mitoribosomal subunits (2), have diverged markedly from their bacterial predecessors by extensive shortening of their ribosomal RNAs (rRNAs) and acquisition of numerous mitochondrial-specific ribosomal proteins (3-6). The initiation of mammalian mitochondrial translation, which involves recruitment of leaderless mRNAs to the 28S subunit and start codon selection in the absence of Shine-Dalgarno sequences (7, 8), is poorly understood.

Mitoribosomes are of high medical interest because aminoglycosides, which are used as antibiotics targeting bacterial ribosomes (9) can also inhibit mitoribosomes, causing severe side effects, such as hearing loss (ototoxicity) (10, 11) in up to 10-20% of patients (10). Furthermore, mitoribosomal mutations play a role in congenital disorders (11, 12), and up-regulation of mitochondrial translation appears to be associated with the development of cancer (13).

Structures of the porcine (14) and human (15) mitoribosomal 39S subunits at 3.4 Å resolution provided detailed insight into their architecture and function, including the architectural replacement of the 5S rRNA by a tRNA molecule. However, structural information on the mammalian 28S small mitoribosomal subunit is currently limited to fitting of homology models into lower resolution reconstructions (16). Here, we present the complete structure of the porcine 28S small mitoribosomal subunit at 3.6 Å resolution and an atomic model of the entire 55S mitoribosome in complex with mRNA and tRNAs based on a 3.8 Å cryo-electron microscopic (cryo-EM) reconstruction.

## **Structure of the mammalian 55S mitoribosome**

To determine the structure of the 55S mitoribosome, we used a previously collected cryo-EM dataset (14). We first calculated a map of the 28S subunit at 3.6 Å resolution by focused classification and alignment (Fig. S1A, B), which allowed us to build a structure for >99% of the 12S rRNA nucleotides and all 30 proteins of the 28S mitoribosomal subunit (Figs. S1B-H, S2A-C; Tables S1, S2, S3). Two proteins, mS27 and mS39, were modeled as poly-serines (Table S3) due to lower local resolution (Fig. S1C, D). This structure was then combined with our previously determined structure of the 39S mitoribosomal subunit at 3.4 Å resolution (14) to build, refine, and validate a complete atomic model of the 55S mitoribosome (Fig. 1A, B; Fig. S2D-F; Tables S2, S3, S4) based on a 3.8 Å cryo-EM map (Fig. S3; Supplementary Text).

The mammalian 55S mitoribosome has a strikingly different appearance compared to the bacterial 70S ribosome (5, 17). The reduced rRNA is limited to the innermost core of the ribosome, whereas numerous proteins cover the surface of the ribosome almost entirely and extend far away from the core.

The structure reveals that in mitochondria, the subunits interact less extensively than in bacteria (Fig. 1C, D; Fig. S4; Table S5; for nomenclature see Materials and Methods) and that many bridges are formed by mitochondrial-specific RNA and protein elements (Fig. S4G-L; Table S5; Supplementary Text). The reduction of peripheral contacts in the mitoribosome may lead to increased conformational flexibility of the mitoribosomal subunits, including tilting of the subunits relative to each other (Fig. S3E-G, S5; Supplementary Text).

## **Interactions of tRNAs with the 55S mitoribosome**

The binding sites for the A-site and P-site tRNAs at the subunit interface lack many ribosomal elements present in cytosolic ribosomes (14, 15, 17), which are compensated for by unique structural features of the mammalian

mitoribosome (Table S6). The 39S subunit interactions with the highly variable mitochondrial tRNA elbows, which could not be modeled because the mitoribosomes in our sample contain a mixture of all mitochondrial tRNAs, have been weakened by the loss of ribosomal protein uL5 in the P-site and bL25 and the A-site finger (rRNA helix H38) in the A-site (Fig. 2A, B) (14, 15). Additionally, uS13, which binds to the anticodon stem loops (ASLs) in bacterial ribosomes (18), has been lost from the 28S subunit (Fig. 2A, C). A unique structural element of the mammalian mitoribosome, the P-site finger (5, 14), compensates for some of these missing interactions, as it extends from the CP of the 39S subunit and is inserted between the A- and P-site tRNAs. The P-site finger seems to play a critical role in positioning of both tRNAs in the active site, as it binds to the D-stem junction and the T-stem of the P-site tRNA and the D-stem of the A-site tRNA (Fig. 2D-F).

### **Structure of the 28S subunit**

The structure of the 28S subunit reveals the folds and locations of its 30 ribosomal proteins, 15 of which are specific to mitoribosomes (Fig. 3A, B; Fig. S6A), in agreement with our CX-MS crosslinking data (Fig. S6B-D; Table S1). The 12S rRNA in the 28S subunit is shortened compared to the bacterial 16S rRNA due to the absence of a number of large rRNA helices (Fig. S7). At the 28S subunit head, the rRNA of the beak is almost entirely missing (Fig. S7A-D), while the loss of bacterial h12 near the center of the small subunit body has resulted in the formation of a channel through the 28S subunit (Fig. S7F), which widens into a large cavity below mS22 on the solvent side of the subunit (Fig. S7G). The distal end of rRNA helix h44 at the subunit interface is partially unwound to position its tip similarly to the tip of h44 in bacteria and in proximity to mS27, even though the mitoribosomal h44 is 18 nt shorter. This unwound segment no longer recognizably forms an A-form RNA helix and appears flexible in our cryo-EM maps (Figs. S2B).

Three homologs of bS18, previously termed MRPS18A, B, and C (19, 20), localize to three distinct sites in the mammalian mitoribosome (Fig. S8A, B), contrary to the initial assumption that all of them occupy a single site in a

mutually exclusive fashion (16, 19). bS18m (MRPS18C) binds to the same site as bacterial bS18, mS40 (MRPS18B) binds to a novel location of the 28S subunit (Fig. S8A), and mL66 (MRPS18A) binds to the 39S subunit (14, 15). All three mitochondrial bS18 homologs are zinc-binding proteins, but one of the zinc-coordinating residues is missing in bS18m (MRPS18C) and mL66 (MRPS18A), and is instead provided in *trans* by uL10m and bS6m, respectively (Fig. S8C-G). These unusual interactions where two protein chains coordinate the same zinc ion may have evolved to stabilize the folds of rapidly evolving mitoribosomal proteins and their quaternary interactions.

### **The mRNA channel**

The structure of the 28S subunit reveals the molecular details of the highly remodeled entry and exit regions of the mitoribosomal mRNA channel (Fig. 4A). The mRNA entry site is surrounded by proteins uS3m, uS5m, mS33, and mS35. An extension of uS5m lines a part of the mRNA entry path and connects the 28S subunit body to the head (Fig. 4B), thus forming a latch across the mRNA channel entrance. Therefore, during translation initiation, the mRNA may need to be threaded through the opening defined by the 12S rRNA and uS5m, unless the uS5m latch dissociates (Fig. 4B). A dynamic role of this protein in mRNA binding is supported by a comparison of two reconstructions of particle subclasses, one with and one without bound mRNA and tRNAs (Fig. S1A), indicating that although the contact points of the latch to the 28S body and head remain intact, the helical part of the extension of uS5m that encircles the mRNA entry path is disordered in the complex devoid of tRNAs, but ordered in the complex containing mRNA and tRNAs (Fig. 4C, D).

The pentatricopeptide repeat (PPR)-containing protein mS39 is located close to the mRNA channel entry (Fig. 4A, B) and forms part of the structure previously termed the mRNA gate (5). Remaining difference density, possibly attributable to mRNA, extends towards the PPR domain of mS39 (Fig. 4C). Consistent with the described role of PPR repeats in single stranded RNA

binding (21), mS39 may therefore bind and guide mitochondrial mRNAs into the mitoribosomal mRNA channel.

Near the decoding center, where mRNA codon-tRNA anticodon base pairing is monitored to select cognate tRNAs (22), density for the mRNA and the well-ordered ASLs of the bound A- and P-site tRNAs can be directly visualized in our cryo-EM map (Fig. 4E, F). The conformation of the mRNA in this region is similar to bacterial ribosomes (Fig. S9). Even though the density in our cryo-EM map is an average of all mRNA and tRNA species, the location of base pairs formed between the tRNAs and the mRNA can be directly observed (Fig. 4F). Our structure indicates that the mechanism of decoding of the 28S subunit is highly conserved, including the interactions of the flipped-out bases A918 and A919 as well as base G256 (corresponding to bacterial nucleotides A1492, A1493, and G530, respectively (22)) with the minor groove of the codon-anticodon helix (Fig. 4G).

The recognition of leaderless mitochondrial mRNAs (7) by the 28S subunit during initiation does not rely on base pairing with rRNA (23). Consequently, the exit region of the mitoribosomal mRNA channel has very different features compared to bacteria, and the 12S rRNA lacks the anti-Shine-Dalgarno sequence. The exit of the mitoribosomal mRNA channel is encircled by the conserved proteins uS7m, uS11m, bS18m, bS21m, and the mitochondrial-specific protein mS37 (Fig. 4H). It has been suggested that respiratory chain failure prevents formation of two conserved regulatory disulfide bridges in Mrp10, the yeast homolog of mS37 (Fig. 4H), leading to degradation of the protein and mitochondrial translation shutdown (24). This suggests that impaired assembly of the mRNA exit channel may play a role in this process.

### **The guanine nucleotide-binding protein of the 28S subunit**

Mammalian mitoribosomes bind guanine nucleotides with high affinity (25). The protein that confers this activity has been identified as mS29 (also termed DAP3 for death-associated protein 3) (26, 27). Our structure reveals that mS29 forms part of the small subunit head (Figs. 3A, 5A) and interacts with

the 12S rRNA, uS7m, uS9m, and mS35 (Fig. 5A), burying a large surface area of approx. 3400 Å<sup>2</sup>, in addition to its involvement in intersubunit bridge formation with the 39S subunit (Fig. S4G). The topology of the β-sheet in the nucleotide binding domain (NBD) and the presence of a C-terminal α-helical bundle (Fig. S10A) indicate that mS29 is structurally related to members of the AAA+ ATPase-family (28). In the mS29 nucleotide binding pocket, one of two conserved acidic residues in the Walker B-motif is replaced by a glycine (Fig. S10C) (28). This is typical for NACHT-NTPase subfamily of STAND ATPases, which perform a variety of functions, including regulation of apoptosis in metazoans (29), and where preference of guanine- over adenine-nucleotides also occurs (29).

In comparison to the AAA+ ATPase core, mS29 contains two sequence insertions that participate in rRNA binding and intersubunit bridge formation, and additionally its N-terminus forms a compact α<sub>2</sub>β<sub>2</sub>-domain that covers the nucleotide binding pocket (Fig. S10B). Our density indicates that a nucleotide, likely GDP, is bound to mS29 in our sample (Fig. S10D). Due to the close proximity of the mS29 nucleotide-binding pocket to the rRNA binding interface (Fig. S10C), the presence of a γ-phosphate in GTP-bound mS29 might induce conformational rearrangements of rRNA-binding residues that interfere with the binding of mS29 to the 28S subunit.

mS29 has been shown to be phosphorylated *in vivo* (30). Because the proposed phosphorylation sites map to the region involved in formation of intersubunit bridges B1b-B1d (Fig. 5B), mS29 phosphorylation may affect intersubunit bridge formation, which might provide a means of regulating the activity of the mammalian mitoribosome.

### **Insights into antibiotic binding and human pathologies**

Aminoglycosides target the bacterial 30S subunit by binding to a pocket in rRNA helix 44 near the ribosomal A-site and the decoding center (9, 31, 32) (Fig. 6A). Overlaying our structure of the 28S subunit with structures of the bacterial 30S subunit in complex with the aminoglycosides paromomycin (18)

and gentamicin (33) reveals that one end of the binding pocket of these aminoglycosides is widened in the 28S subunit because of the presence of the A916-C854 and C917-C853 mismatches (Fig. 6B), in agreement with sequence analysis (34). In spite of these structural differences, some aminoglycosides can still bind to the decoding site of the small subunit of the mitoribosome, which can lead to hearing loss (ototoxicity), particularly in patients with the A916G or C854U mutation in the 12S rRNA (A1555G and C1494T in the human mitochondrial genome (34)), which occur in roughly 0.2-0.3 % of the general population (35). These mutations revert the A916-C854 mismatch found in wild-type mitoribosomes to a bacterial-like state with a Watson-Crick base pair at this position. The aminoglycoside apramycin binds to the 30S subunit in the same region, but exhibits lower toxicity towards mitochondrial translation even in the presence of sensitizing mutations (36). Apramycin is embedded less deeply in the rRNA compared to other aminoglycosides (36), likely making its binding more dependent on the stacking interaction of its bicyclic ring system with the bacterial G1491-C1409 base pair, which is replaced by the C917-C853 mismatch in the mitoribosomal 12S rRNA (Fig. 6B).

Several mutations in mitoribosomal proteins have been identified in human pathologies. A nonsense mutation in bS16m (MRPS16) that leads to death soon after birth (37) and two point mutations in mS22 (MRPS22) (38, 39) affect the lower body domain of the 28S subunit (Fig. 6C, D) where they may impair its assembly (40).

The atomic structures presented here pave the way to a mechanistic understanding of human mitochondrial translation and associated pathologies, and will also facilitate rational design of antimicrobials and compounds that block cancer cell proliferation.

## References and Notes

1. L. Sagan, On the origin of mitosing cells. *J. Theor. Biol.* **14**, 255-274 (1967).
2. T. W. O'Brien, The general occurrence of 55 S ribosomes in mammalian liver mitochondria. *J. Biol. Chem.* **246**, 3409-3417 (1971).
3. E. C. Koc *et al.*, Identification and characterization of CHCHD1, AURKAIP1, and CRIF1 as new members of the mammalian mitochondrial ribosome. *Front. Physiol.* **4**, 183 (2013).
4. E. Desmond, C. Brochier-Armanet, P. Forterre, S. Gribaldo, On the last common ancestor and early evolution of eukaryotes: reconstructing the history of mitochondrial ribosomes. *Res. Microbiol.* **162**, 53-70 (2011).
5. M. R. Sharma *et al.*, Structure of the mammalian mitochondrial ribosome reveals an expanded functional role for its component proteins. *Cell* **115**, 97-108 (2003).
6. B. J. Greber *et al.*, Architecture of the large subunit of the mammalian mitochondrial ribosome. *Nature* **505**, 515-519 (2014).
7. J. Montoya, D. Ojala, G. Attardi, Distinctive features of the 5'-terminal sequences of the human mitochondrial mRNAs. *Nature* **290**, 465-470 (1981).
8. C. N. Jones, K. A. Wilkinson, K. T. Hung, K. M. Weeks, L. L. Spremulli, Lack of secondary structure characterizes the 5' ends of mammalian mitochondrial mRNAs. *RNA* **14**, 862-871 (2008).
9. D. N. Wilson, Ribosome-targeting antibiotics and mechanisms of bacterial resistance. *Nat. Rev. Microbiol.* **12**, 35-48 (2014).
10. J. Xie, A. E. Talaska, J. Schacht, New developments in aminoglycoside therapy and ototoxicity. *Hear. Res.* **281**, 28-37 (2011).
11. A. Rötig, Human diseases with impaired mitochondrial protein synthesis. *Biochim. Biophys. Acta.* **1807**, 1198-1205 (2011).
12. S. B. Vafai, V. K. Mootha, Mitochondrial disorders as windows into an ancient organelle. *Nature* **491**, 374-383 (2012).
13. F. Sotgia *et al.*, Mitochondria "fuel" breast cancer metabolism: fifteen markers of mitochondrial biogenesis label epithelial cancer cells, but are excluded from adjacent stromal cells. *Cell Cycle* **11**, 4390-4401 (2012).
14. B. J. Greber *et al.*, The complete structure of the large subunit of the mammalian mitochondrial ribosome. *Nature* **515**, 283-286 (2014).
15. A. Brown *et al.*, Structure of the large ribosomal subunit from human mitochondria. *Science* **346**, 718-722 (2014).
16. P. S. Kaushal *et al.*, Cryo-EM structure of the small subunit of the mammalian mitochondrial ribosome. *Proc. Natl. Acad. Sci. U. S. A.*, (2014).
17. M. M. Yusupov *et al.*, Crystal structure of the ribosome at 5.5 Å resolution. *Science* **292**, 883-896 (2001).
18. R. M. Voorhees, A. Weixlbaumer, D. Loakes, A. C. Kelley, V. Ramakrishnan, Insights into substrate stabilization from snapshots of the peptidyl transferase center of the intact 70S ribosome. *Nat. Struct. Mol. Biol.* **16**, 528-533 (2009).

19. E. C. Koc, W. Burkhart, K. Blackburn, A. Moseley, L. L. Spremulli, The small subunit of the mammalian mitochondrial ribosome. Identification of the full complement of ribosomal proteins present. *J. Biol. Chem.* **276**, 19363-19374 (2001).
20. T. Suzuki *et al.*, Proteomic analysis of the mammalian mitochondrial ribosome. Identification of protein components in the 28 S small subunit. *J. Biol. Chem.* **276**, 33181-33195 (2001).
21. A. Filipovska, O. Rackham, Pentatricopeptide repeats: modular blocks for building RNA-binding proteins. *RNA Biol.* **10**, 1426-1432 (2013).
22. J. M. Ogle *et al.*, Recognition of cognate transfer RNA by the 30S ribosomal subunit. *Science* **292**, 897-902 (2001).
23. J. Shine, L. Dalgarno, The 3'-terminal sequence of Escherichia coli 16S ribosomal RNA: complementarity to nonsense triplets and ribosome binding sites. *Proc. Natl. Acad. Sci. U. S. A.* **71**, 1342-1346 (1974).
24. S. Longen, M. W. Woellhaf, C. Petrunger, J. Riemer, J. M. Herrmann, The disulfide relay of the intermembrane space oxidizes the ribosomal subunit mrp10 on its transit into the mitochondrial matrix. *Dev Cell* **28**, 30-42 (2014).
25. N. D. Denslow, J. C. Anders, T. W. O'Brien, Bovine mitochondrial ribosomes possess a high affinity binding site for guanine nucleotides. *J. Biol. Chem.* **266**, 9586-9590 (1991).
26. E. C. Koc *et al.*, A new face on apoptosis: death-associated protein 3 and PDCD9 are mitochondrial ribosomal proteins. *FEBS Lett.* **492**, 166-170 (2001).
27. T. Miyazaki, J. C. Reed, A GTP-binding adapter protein couples TRAIL receptors to apoptosis-inducing proteins. *Nat. Immunol.* **2**, 493-500 (2001).
28. J. P. Erzberger, J. M. Berger, Evolutionary relationships and structural mechanisms of AAA+ proteins. *Annu. Rev. Biophys. Biomol. Struct.* **35**, 93-114 (2006).
29. D. D. Leipe, E. V. Koonin, L. Aravind, STAND, a class of P-loop NTPases including animal and plant regulators of programmed cell death: multiple, complex domain architectures, unusual phyletic patterns, and evolution by horizontal gene transfer. *J. of Mol. Biol.* **343**, 1-28 (2004).
30. J. L. Miller, H. Koc, E. C. Koc, Identification of phosphorylation sites in mammalian mitochondrial ribosomal protein DAP3. *Protein Sci.* **17**, 251-260 (2008).
31. A. P. Carter *et al.*, Functional insights from the structure of the 30S ribosomal subunit and its interactions with antibiotics. *Nature* **407**, 340-348 (2000).
32. D. Moazed, H. F. Noller, Interaction of antibiotics with functional sites in 16S ribosomal RNA. *Nature* **327**, 389-394 (1987).
33. M. A. Borovinskaya *et al.*, Structural basis for aminoglycoside inhibition of bacterial ribosome recycling. *Nat. Struct. Mol. Biol.* **14**, 727-732 (2007).
34. T. R. Prezant *et al.*, Mitochondrial ribosomal RNA mutation associated with both antibiotic-induced and non-syndromic deafness. *Nat. Genet.* **4**, 289-294 (1993).

35. M. Bitner-Glindzicz *et al.*, Prevalence of mitochondrial 1555A-G mutation in European children. *N. Engl. J. Med.* **360**, 640-642 (2009).
36. T. Matt *et al.*, Dissociation of antibacterial activity and aminoglycoside ototoxicity in the 4-monosubstituted 2-deoxystreptamine apramycin. *Proc. Natl. Acad. Sci. U. S. A.* **109**, 10984-10989 (2012).
37. C. Miller *et al.*, Defective mitochondrial translation caused by a ribosomal protein (MRPS16) mutation. *Ann. Neurol.* **56**, 734-738 (2004).
38. P. Smits *et al.*, Mutation in mitochondrial ribosomal protein MRPS22 leads to Cornelia de Lange-like phenotype, brain abnormalities and hypertrophic cardiomyopathy. *Eur. J. Hum. Genet.* **19**, 394-399 (2011).
39. A. Saada *et al.*, Antenatal mitochondrial disease caused by mitochondrial ribosomal protein (MRPS22) mutation. *J. Med. Genet.* **44**, 784-786 (2007).
40. M. Emdadul Haque, D. Grasso, C. Miller, L. L. Spremulli, A. Saada, The effect of mutated mitochondrial ribosomal proteins S16 and S22 on the assembly of the small and large ribosomal subunits in human mitochondria. *Mitochondrion* **8**, 254-261 (2008).

**Acknowledgments** EM data was collected at the ScopeEM facility of ETH Zurich. We thank Peter Tittmann (ScopeM) for support and Jan Erzberger for discussions. This work was supported by the Swiss National Science Foundation (SNSF), the National Center of Excellence in Research (NCCR) Structural Biology and RNA & Disease programs of the SNSF, the European Research Council grant 250071 under the European Community's Seventh Framework Programme (to N.B.), the Commission of the European Communities through the PROSPECTS consortium (EU FP7 projects 201648, 233226) (R.A.), and the European Research Council (ERC-2008-AdG 233226) (R.A.). The 3.6 Å cryo-EM map of the 28S mitoribosomal subunit and the 3.8 Å cryo-EM map of the 55S mitoribosome have been deposited with accession codes EMD-2913 and EMD-2914. Coordinates of the refined 28S subunit and the 55S mitoribosome in the canonical state have been deposited with PDB codes 5AJ3 (28S) and 5AJ4, 5AJ6 and 5AJ7 (55S). A PyMol script for display of the 55S mitoribosome is available from the Ban Lab website ([http://www.mol.biol.ethz.ch/groups/ban\\_group/](http://www.mol.biol.ethz.ch/groups/ban_group/)).

## Supplementary Materials

Materials and Methods

Supplementary Text

Figures S1 to S10

Tables S1 to S7

References (41-67)

Additional Data Table S1 as a separate spread sheet file

## Figure Legends

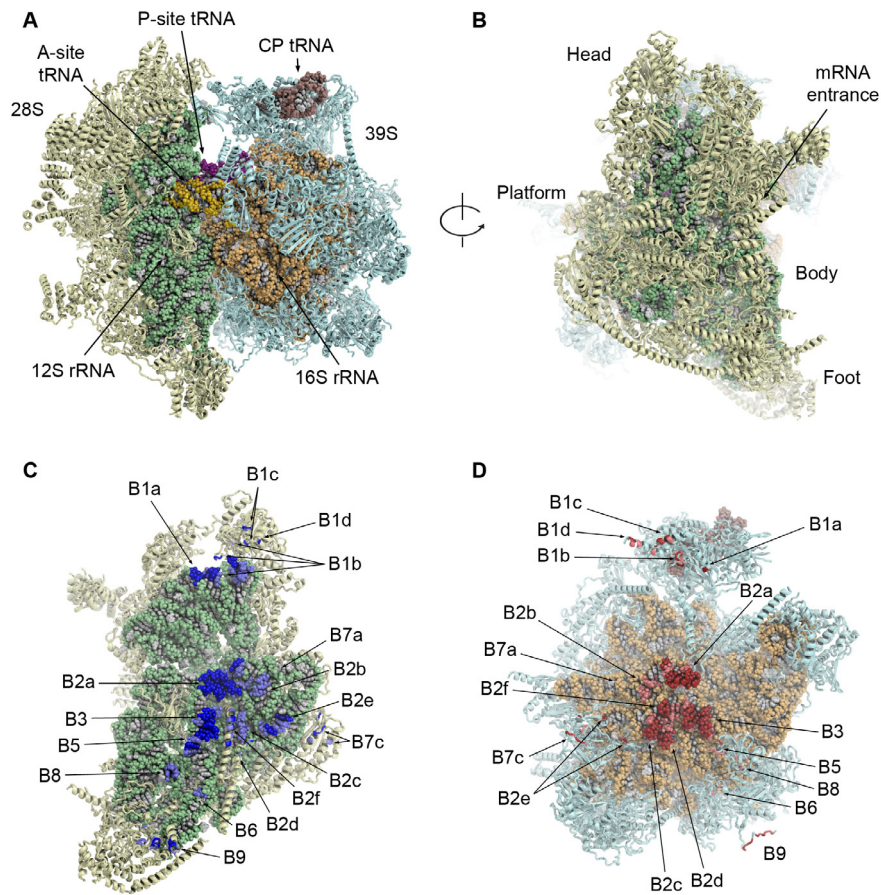


**Figure 1. Overall structure of the 55S mitoribosome. (A, B)** Structure of the 55S mitoribosome. 39S subunit proteins blue, 16S rRNA orange, CP tRNA brown, 28S subunit proteins pale yellow, 12S rRNA light green, P-site tRNA purple, A-site tRNA yellow. **(C, D)** Intersubunit bridges in the 55S mitoribosome. Contact surfaces (distance  $< 4 \text{ \AA}$ ) and surfaces in close proximity ( $< 6 \text{ \AA}$ ) are colored in blue and pale blue **(C)** or red and pale red **(D)**, respectively, and labeled with the bridge number.

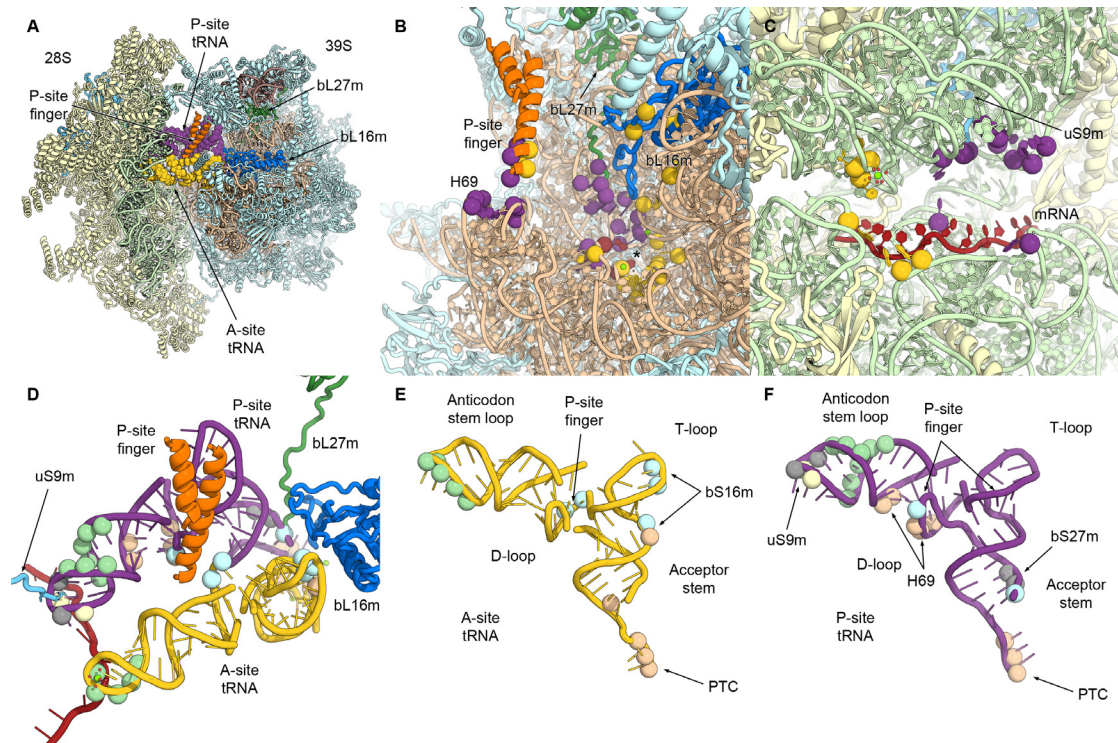


**Figure 2. Interactions of tRNAs in the 55S mitoribosome.** (A) Overview of the 55S mitoribosome. Colors as in Fig. 1, but with proteins approaching the A- and P-site tRNAs highlighted (bL16m blue, bL27m green, P-site finger orange, uS9m cyan). (B, C) View of the 39S (B) and 28S (C) tRNA binding sites (A- and P-site tRNA contacts yellow and purple; PTC indicated by asterisk). (D) tRNA-protein interactions in the 55S mitoribosome (contacts to 16S rRNA brown, 12S rRNA light green, 39S proteins cyan, 28S proteins pale yellow, residues contacting both rRNA and proteins grey). (E, F) A- and P-site tRNAs displayed as in (D), with major tRNA domains labeled and interacting mitoribosomal components indicated.

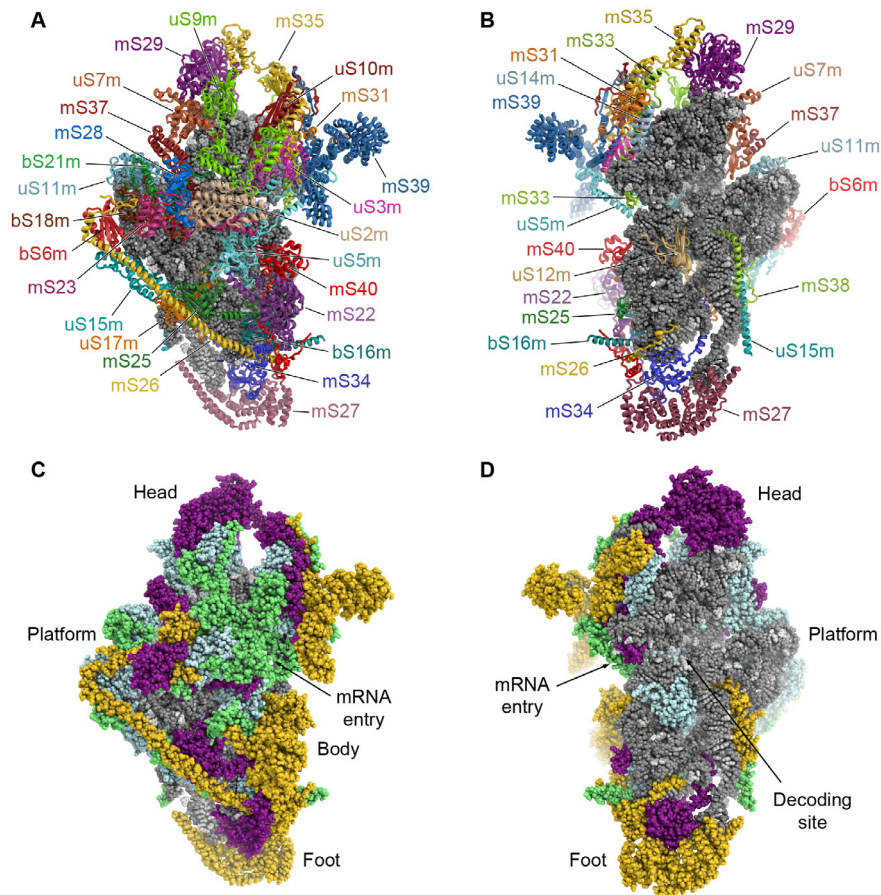


**Figure 3. Overall structure of the 28S subunit.** (A, B) Locations of proteins in the 28S subunit (A, solvent side; B, subunit interface side). (C, D) 28S subunit (oriented as in A, B) with ribosomal proteins colored according to conservation (grey: 12S rRNA; cyan: proteins conserved in bacteria, mitoribosomal extensions green; purple: proteins shared between fungal and mammalian mitoribosomes; yellow: proteins not present in fungal mitoribosomes).

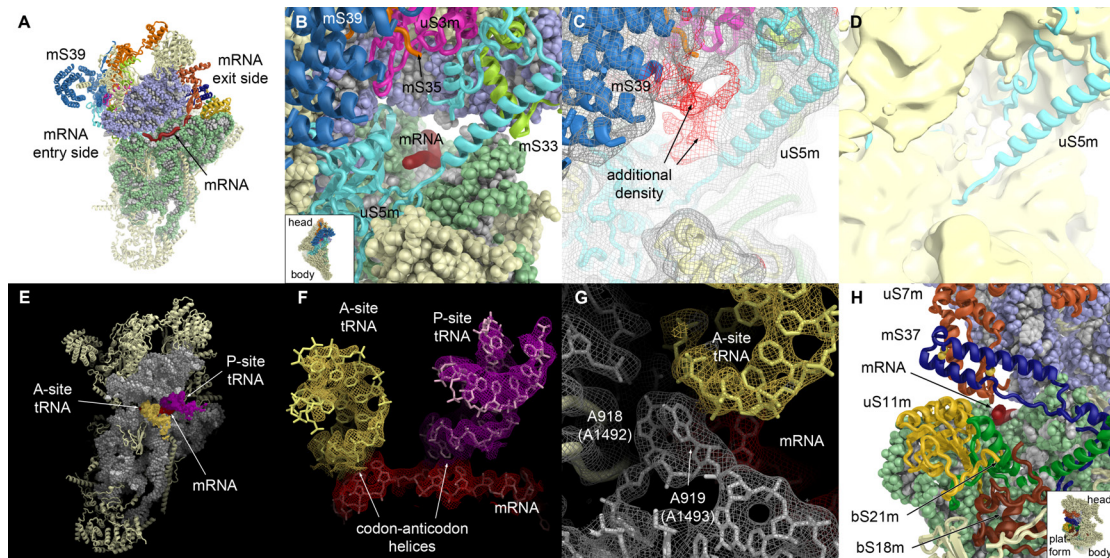


**Figure 4. The mRNA binding channel of the 28S subunit.** (A) Subunit interface view of the 28S subunit (proteins surrounding the mRNA entry and exit sites colored). (B) uS5m (cyan) forms a latch across the entrance of the mRNA channel (mRNA dark red). (C) Additional density (red) is visible near the mRNA entry path in a particle subclass with a well-ordered mRNA gate. (D) The mRNA entry site of the 28S without bound mRNA and tRNAs (yellow surface) lacks density for the uS5m latch (cyan). (E) Density for mRNA (red) and tRNAs (P-site purple, A-site yellow). (F) Close-up view of the mRNA and tRNA density. (G) Conservation of the decoding center with flipped-out A918 and A919. (H) The exit of the mRNA channel (colors as in A, with disulfide bridges in mS37 shown as yellow spheres).

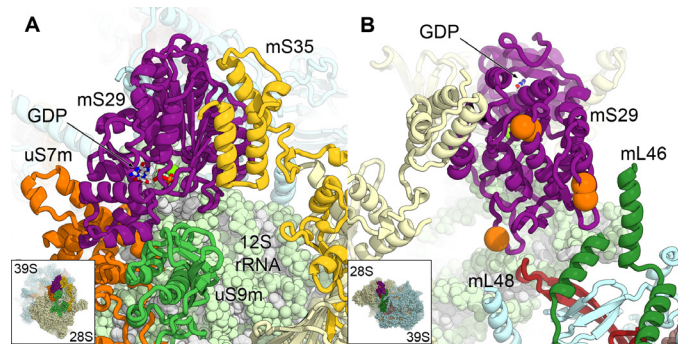


**Figure 5. The guanine-nucleotide binding protein mS29. (A)** Position of mS29 (purple, GDP white) in the head domain of the 28S subunit. **(B)** Putative mS29 phosphorylation sites (orange spheres) near subunit bridges B1b and B1c (mL46 green, mL48 dark red).

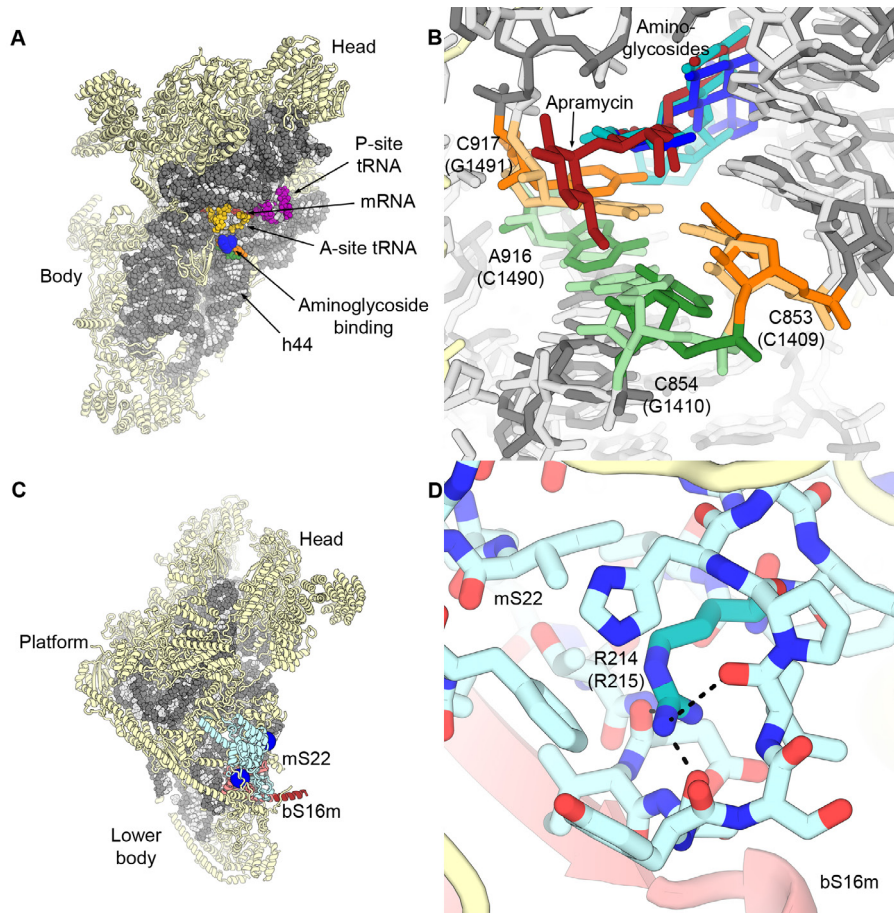


**Figure 6. Aminoglycoside binding to the 28S subunit and mapping of mitoribosomal protein mutations.** (A) 28S subunit with aminoglycoside binding region near the A-site in blue (A- and P-site tRNA fragments gold and purple, respectively). (B) Superposition of the structures of paromomycin (cyan), gentamycin (blue), and apramycin (red) bound to the bacterial 30S subunit (18, 33, 36). Positions of relevant sequence differences between mammalian mitoribosomes and bacterial ribosomes (18) shown in orange and green. (C) Location of human mutations in mS22 (light blue, affected residues as blue spheres) and bS16m (red, helix truncated by a nonsense-mutation dark red). (D) Location and environment of mS22 residue R214 (R215H mutation in humans).